Y. Liu, G. Aldan, X. Huang, M. Hao (2023) *Single-phase static immersion cooling for cylindrical lithium-ion battery module*, **Applied Thermal Engineering**, 121184. https://doi.org/10.1016/j.applthermaleng.2023.121184

Single-phase static immersion cooling for cylindrical lithium-ion battery module

Yanhui Liu[a,b], Gulzhan Aldan[a], Xinyan Huang[a,b,*], Menglong Hao[c,*]

[a] *Department of Building Environment and Energy Engineering, The Hong Kong Polytechnic University, Hong Kong SAR, China*

[b] *The Hong Kong Polytechnic University Shenzhen Research Institute, Shenzhen, China*

[c] *Key Laboratory of Energy Thermal Conversion and Control of Ministry of Education, School of Energy and Environment, Southeast University, Nanjing, China*

** Corresponding to xy.huang@polyu.edu.hk (X. Huang); haom@seu.edu.cn (M. Hao)*

Abstract

The single-phase immersion cooling is an emerging technology for battery thermal management. Both static- or forced-flow working fluids can be adopted, while the advantages of the static mode are less complexity and low cost. This work proposes a static flow-based immersion cooling method for a six-cell cylindrical Li-ion battery module. The effectiveness of the proposed immersion cooling system is studied at different current rates and compared with conventional air-cooling methods. Experiments find that the maximum cell temperature (T_{max}) appears at the end of discharge, and it increases with the C-rate. The proposed immersion cooling system can limit the T_{max} below 40 °C and temperature gradient within 3 °C at 3C discharge, exhibiting a superior cooling capability over air cooling. The three-dimensional numerical model has been established to further analyze and optimize the performance of the proposed immersion cooling system. Modelling suggests that immersion cooling has a maximum cooling rate of 2.7 W for the cell with the highest temperature, which is 50% higher than the cooling rate of the forced air-cooling system. In addition, the effects of ambient temperature and liquid volume have been numerically investigated. Different cooling regions are defined to evaluate the thermal-management performance of the immersion cooling system. Finally, the cooling efficiency of three different fluids is compared in a 100-cell battery module, which can provide valuable information for battery thermal management and scientific guidelines for applying immersion cooling for batteries in operation.

Keywords: *battery thermal management; direct liquid cooling; static mode; battery safety*

Nomenclature

Symbols		θ	temperature difference [°C]
A	surface area [m^2]	μ	dynamic viscosity [Pa-s]
c	specific heat [J/(kg·K)]	ρ	density [kg/m^3]
h	heat transfer coefficient [$W/(m^2 \cdot K)$]		
k	thermal conductivity [W/(m·K)]	**Subscripts**	
m	mass [g]	a	ambient
$\dot{q}$	heating/cooling rate [W]	c	cooling
$\dot{q}'''$	volumetric heat generation rate [W/m^3]	i	cell number
Q	total amount of heat [J]	*LIB*	lithium-ion battery
r	repeat test [-]	*max*	maximum
t	time [s]		
T	temperature [°C]	**Abbreviations**	
ΔT	Temperature difference [°C]	*BTMS*	battery thermal management system
v	velocity [m/s]	*CC-CV*	constant current - constant voltage
		DOD	depth of discharge
Greeks		*LIB*	lithium-ion battery
δ	liquid-battery volume ratio [-]	*PCM*	phase change material

1. Introduction

The Lithium-ion battery (Li-ion battery or LIB) is a promising energy-storage technology due to its high energy density and low self-discharge rate. It has been extensively used in electronic devices, electric vehicles, and energy storage systems, playing a vital role in achieving global carbon neutrality. However, the working performance of the LIB is susceptible to its temperature [1,2]. The optimal operating temperature for the LIB should be within 20 ~ 40 °C, with a temperature gradient of less than 5 °C [3]. A high operating temperature would accelerate the battery ageing and degradation, or even trigger thermal runaway [4] and fire propagation [5,6]. Thus, an effective battery thermal management system (BTMS) is essential to maintain the battery temperature in a proper range to reduce thermal safety issues and maximize the battery lifetime [7–9].

In recent years, attention has been paid to exploring and selecting suitable BTMS for specific battery modules [10–16]. Air cooling, liquid cooling, and phase change material (PCM) cooling are three common cooling strategies in BTMS. Air cooling system (with natural or forced convection) has a simple design, low cost, and high commercial maturity, but its low cooling efficiency and temperature inhomogeneity cause serious fire and safety concerns [17–19]. The PCM based cooling has a higher efficiency due to its much higher latent heat [20–22]. However, the material used in this type of cooling usually has high flammability, relatively low thermal conductivity, and is prone to leakage [23]. Alternatively, liquid cooling is one of the most widely used cooling methods in the current BTMS due

to the high heat transfer coefficient and specific heat capacity of the adopted coolants [24–26]. From the perspective of contact mode, the liquid cooling of BTMS can be classified as indirect cooling and direct cooling. In the indirect liquid cooling system, the coolants, usually water or ethylene glycol, flow in the metal tubes or plates placed in direct contact with the battery and indirectly remove the heat from the battery surface [27–29]. Due to the limited space in the battery pack, the structure of cooling tubes or plates could be complex. The cooling performance of indirect liquid cooling highly depends on various factors such as battery shape [27,30], cooling plate design [31], coolant flow [32], and so on. Although a lot of research has been devoted to optimizing the performance of the indirect liquid cooling system, its extra energy consumption related to liquid pumping and the complexity of the system remain the major issues.

In the BTMS with direct liquid cooling, batteries are immersed in the dielectric liquid, ensuring direct contact with the coolant. Direct liquid immersion cooling utilizes sensible (single-phase cooling) or latent heat (two-phase cooling) of the liquid coolants to dissipate heat generated by the battery cells, which leads to a superior cooling performance [33]. Typical candidate dielectric liquids include fluorinated fluids, mineral oils, esters, and water-glycol mixtures. As some of the fluid candidates are flame-retardant, immersion cooling also has enormous potential to prevent batteries from thermal runaway and its propagation [34,35]. Thus, direct liquid cooling has drawn attention to all types of pouch [36–38], prismatic [39–41], and cylindrical batteries [42–51]. Particularly, immersion cooling for cylindrical cells has a premier performance due to a large surface-volume ratio [52]. According to the flow mode and phase state, the different types of complete immersion cooling systems are illustrated in Fig. 1.

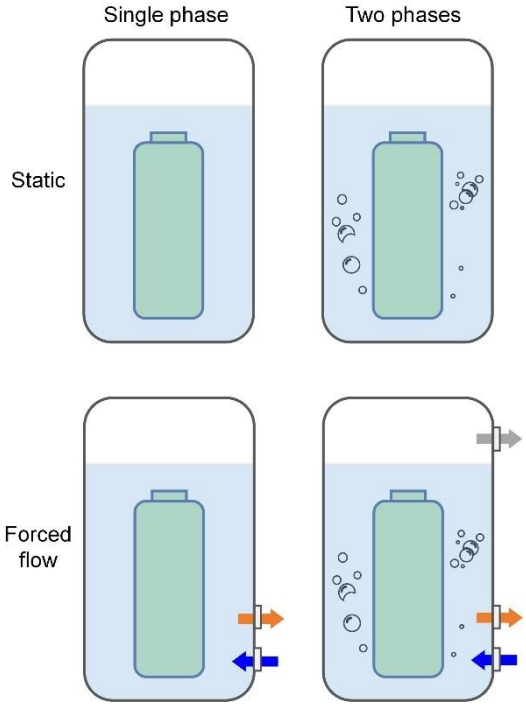

Fig. 1. Schematic diagram for different types of complete immersion cooling systems [8].

Generally, the two-phase immersion cooling technique submerges the battery in coolants that possess a low boiling point. When the cell temperature exceeds this boiling point, the resultant heat will cause the adjacent liquid to vaporize, thereby cooling the battery rapidly. The condensed liquid is subsequently cycled back into the original liquid bath, completing the cooling cycle. For two-phase immersion cooling, van Gils *et al.* [45] found that the boiling process of liquid can thermally homogenize the cell temperature. Li *et al.* [46] further studied the mechanism of this bubbling process using high-speed photographs and verified the effectiveness of two-phase immersion cooling for a single cell.

Although two-phase immersion cooling shows excellent efficacy in improving the temperature uniformity of the battery module, the condensing process of the two-phase immersion system will cause additional costs. Moreover, Wang *et al*. [47] found that single-phase liquid cooling has more advantages in regulating the maximum temperature of the battery module. Thus, several single-phase immersion cooling systems have gained research interest recently [49–52]. For example, Liu *et al.* [50] designed an oil-immersed BTMS for a cylindrical cell, where the effect of flow rate on its cooling performance was experimentally investigated. Similarly, Jithin and Rajesh [49] adopted single-phase immersion cooling for a 4-cell battery module and numerically studied the cooling performance of three different fluids. However, most single-phase immersion cooling systems use forced flow, while the studies on static mode are limited. Static immersion cooling is low-cost and highly reliable without a complex flow system. More research is needed to investigate the usage of static immersion cooling, especially for use in cylindrical cells with large surface-volume ratios.

This work proposes a static-flow single-phase immersion cooling system and demonstrates it for a 6-cell cylindrical battery module with a parallel connection (6P1S). Its cooling performance is evaluated by experiments of different current rates and compared with conventional air-cooling. Afterwards, a 3D numerical model is established and then validated by experiments. The developed numerical model further explores the effects of ambient temperature and coolant volume on thermal management performance. Finally, a comparative analysis is performed for immersion-cooling BTMS with different coolants in a 100-cell module. This work is a significant addition to the literature, which will provide new insights into liquid-cooling BTMS and deepen our understanding of static-flow immersion cooling systems.

2. Experimental setup

2.1. Battery module and apparatus

The cylindrical cells used in this work were manufactured by Samsung SDI Co., Ltd (ICR18650-22P). Each cell has a diameter of 18 mm and a height of 65 mm (Fig. 2a). The nominal capacity of this cell is 2.2 Ah, and the nominal voltage is 3.6 V. To reduce the experimental uncertainty, cells from the same batch were selected for the cycling tests. As shown in Fig. 2b, six cells were connected in parallel by nickel tabs to form a battery module (6P1S), following the rectangular module shape used in previous

studies [16,53]. The gap between two adjacent cells is 2 mm. The nickel tab has a thickness of 0.5 mm and a width of 7 mm. As presented in Table 1, the nominal capacity of the battery module is 13.2 Ah.

Table 1. Specifications of the battery and tab in this work.

Parameters	Battery cell	Nickle tab
Cathode	$Li(Ni_{1/3}Co_{1/3}Mn_{1/3})O_2$	-
Anode	Graphite	-
Nominal capacity [Ah]	2.2	-
Nominal voltage [V]	3.6	-
Minimum cut-off Voltage [V]	2.75 ± 0.05	-
Maximum cut-off Voltage [V]	4.20 ± 0.05	-
Mass [g]	41.5 ± 0.5	-
Volume [mL]	16.53	-
Density [kg/m^3]	2523	8908
Thermal conductivity [W/(m·K)]	1.2 (radial direction) 34.4 (axial direction)	90
Specific heat [J/(kg·K)]	1145 [54]	502

The experimental setup is illustrated in Fig. 2c. A comparative study was conducted to investigate the thermal management performance between the conventional air-cooling system and the proposed immersion cooling system. For the air-cooling BTMS, an acrylic box (5 mm in thickness) with two small fans was utilized to provide a parallel airflow channel environment. Such a method was adopted in many previous studies [55]. The acrylic box has a length of 300 mm, a width of 150 mm, and a height of 150 mm, so its total volume is 6750 mL. In literature, the inlet air velocities of 0.3-0.6 m/s were always selected for the air-cooling BTMS [56–58].

Table 2. Properties of pure dielectric cooling liquid (Novec-7200).

Formulation	Boiling point [°C]	Density [kg/m^3]	Dynamic viscosity [Pa·s]	Specific heat [J/kg·K]	Thermal conductivity [W/(m·K)]
$C_4F_9OC_2H_5$	76	1430	0.00061	1220	0.068 [41]

In terms of the immersion cooling system, the battery module was submerged in the Novec-7200 engineered fluid (manufactured by 3M) with dimensions of 120 mm × 80 mm × 100 mm. Featured as non-toxic and nonflammable, this engineered liquid has been extensively used as a coolant for electronic devices and data centers. According to the specifications and literature [41], the properties of the pure Novec-7200 are summarized in Table 2. To ensure the experimental repeatability, the acrylic box with engineered fluid was put into a water tank at 22 ± 2 °C to make sure that the liquid external boundary has a constant temperature.

The K-type thermocouple with the 2-mm bead and ± 0.1 °C uncertainty was used to measure the cell temperature (T_{LIB}) and the ambient temperature (T_a). Within the battery module, six thermocouples were fixed at the half height of the cell surface by Teflon tape. This Teflon tape is electrically insulated

and able to withstand a high temperature of 200 °C. To avoid the influence of thermocouples on airflow, the plane formed by the temperature measurement points is parallel to the wind direction, and the tape used to fix the thermocouple should be as small as possible. The proposed immersion cooling BTMS and the conventional air cooling BTMS were connected with the battery testing system (Neware, 5V/100A), as demonstrated in Fig. 2c. A computer was integrated with the battery testing system to perform well-controlled cycling tests at different currents. All temperature information was monitored by a data logger (HIOKI LR8400) with a sampling frequency of 1 Hz.

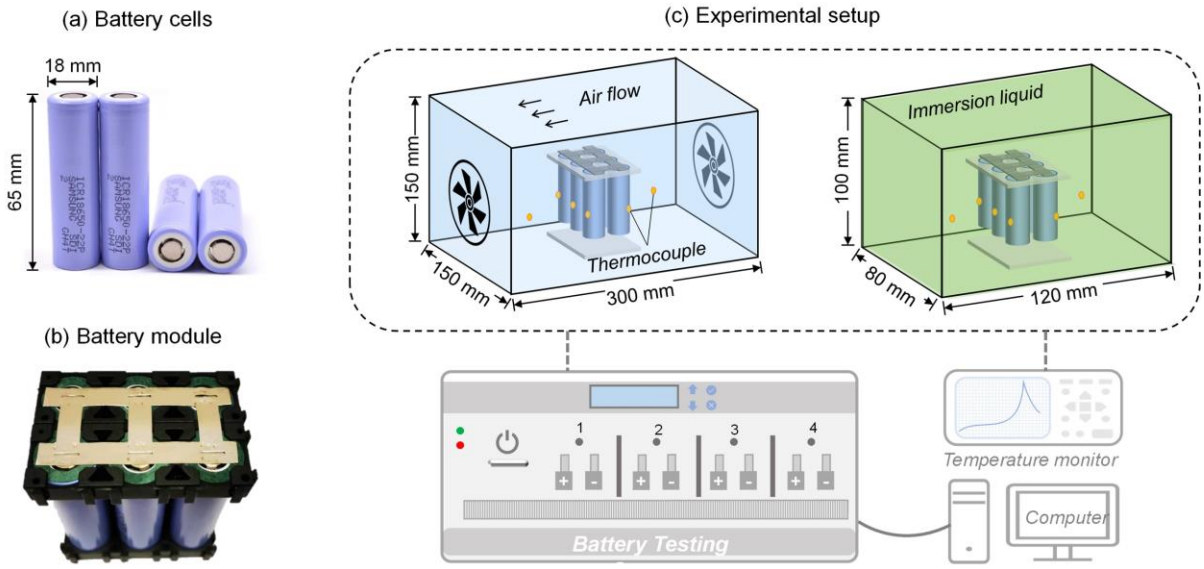

Fig. 2. Photographs of (a) battery cell, (b) battery module, and (c) schematic of the experimental setup (not to scale), where the actual photo is shown in Fig. S1.

2.2. Testing procedures

The charging-discharging tests were conducted to assess the cooling performance of the battery systems. The battery modules underwent several charging-discharging cycles with three C-rates of 1 C (13.2 A), 2 C (26.4 A), and 3 C (39.6 A), respectively. The testing procedures are listed as follows:

(1) Constant Current - Constant Voltage (CC-CV) charge with the cut-off voltage of 4.2 V and cut-off current of 0.05 C;

(2) Rest for 10 min;

(3) Constant Current (CC) discharge until the voltage drops to 2.75 V;

(4) Rest for 10 min;

(5) Repeat the steps of (1)-(4) for twice or three times; and

(6) Final rest until the cell temperature decreases to equilibrium.

The selection of cut-off voltage was based on the battery specifications provided by the manufacturer, where the maximum cut-off voltage for charging is 4.20 ± 0.05 V, and the minimum cut-off voltage for discharging is 2.75 ± 0.05 V. The cycling tests were conducted for the battery module under three different cooling strategies. As shown in Table 3, Group A is the natural convection cooling,

where the fans are switched off. Group B is the forced air-cooling condition, where constant power is supplied to fans to provide an average airflow rate of 0.35 m/s near the battery module. Group C is the proposed immersion cooling condition. To reduce the experimental uncertainty, each test was repeated at least twice. The C-rate in Table 3 represents the measurement of the charge and discharge current with respect to its nominal capacity.

Table 3. Experimental outline of this work.

Group	Cooling strategies	C-rates (C)
A	Natural convection	
B	Forced air cooling	1, 2, and 3
C	Liquid immersion cooling	

3. Numerical methodology

3.1. Measurement of battery heat generation rate

The heat generation rate of cells plays a vital role in simulating the temperature variation of batteries and evaluating the performance of BTMS. In literature, the heat generation rate can be determined by the electrochemical model based on chemical reactions or the empirical model obtained from analysis of cycling data [59]. Since cells exhibit the maximum temperature during the discharging process, the discharging data for cells under natural convection were used to identify the heat generation rate experimentally.

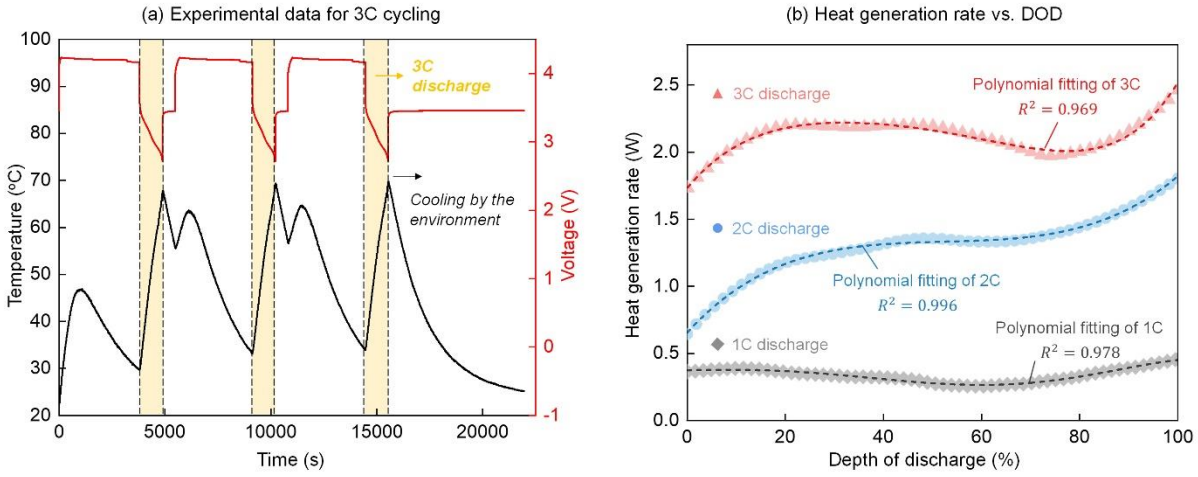

Fig. 3. (a) The temperature evolution for a single cell with 3 C cycling under natural cooling and (b) heat generation rate vs. depth of discharge (DOD) at different discharge rates.

Taking a cell under the 3-C cycling test as an example, Fig. 3a shows the corresponding temperature evolution curve. It mainly contains three CC-CV charging processes and three CC discharging processes. After the final discharging period, the battery cell rested until its temperature decreased to equilibrium. During this period, the temperature decrease was driven by environmental

cooling as

$$m_{LIB}c_{LIB}\frac{dT_{LIB}}{dt} = -h_cA(T_{LIB} - T_a) \tag{1}$$

where m_{LIB} is the mass of the cell, c_{LIB} is the specific heat of the battery, T_{LIB} is the temperature of the cell; t is the time after the final discharge; h_c is the overall heat transfer coefficient; A is the surface area of the cell; and T_a is the ambient temperature, respectively.

Define the temperature difference $\theta = T_{LIB} - T_a$, then $dT_{LIB}/dt = d\theta/dt$. Therefore, Eq. (1) can be rewritten as

$$m_{LIB}c_{LIB}\frac{d\theta}{dt} = -h_cA\theta \tag{2}$$

After separating the variables and integrating Eq. (2), the correlation between the environmental cooling coefficient (h_c) and the cell temperature (T_{LIB}) can be expressed as

$$ln(T - T_a) = \frac{-h_cA}{m_{LIB}c_{LIB}}t + \frac{C}{m_{LIB}c_{LIB}} \tag{3}$$

According to the experimental data, this linear relationship between $ln(T - T_a)$ and t can be plotted, where the slope is $\frac{-h_cA}{m_{LIB}c_{LIB}}$. Finally, the environmental cooling coefficient (h_c) is calculated around 5 W/(m·K). The linear fitting is presented in Fig. S2. On the other hand, the cell temperature during the discharging process should satisfy

$$m_{LIB}c_{LIB}\frac{dT_{LIB}}{dt} = \dot{q} - h_cA(T_{LIB} - T_a) \tag{4}$$

where $\dot{q}$ is the heat generation rate inside the battery. Based on Eq. (4), the calculated heat generation rates varying with the depth of discharge (DOD) are summarized and fitted in Fig. 3b. Apparently, the heat generation rate increases with the discharging rate. For example, the average heating rate of 2-C discharge is about 3 times as much as that at 1-C discharge. According to the empirical heat generation model in literature, the 5th polynomial fitting is adopted in this work [60]. The expression for the heat generation rate is written as

$$\dot{q} = a_o + a_1t + a_2t^2 + a_3t^3 + a_4t^4 + a_5t^5 \tag{5}$$

In this work, the cases with a high C-rate of 3 C will be numerically investigated, and the polynomial coefficients are $a_o = 1.73$, $a_1 = 4.42 \times 10^{-3}$, $a_2 = -1.55 \times 10^{-5}$, $a_3 = 2.85 \times 10^{-8}$, $a_4 = -3.01 \times 10^{-11}$, and $a_5 = 1.35 \times 10^{-14}$, respectively. The R^2 for the curvilinear relationship indicates the reliability of the fitted model.

3.2. Governing equations for numerical model

To numerically investigate the efficacy of immersion cooling and optimize the proposed BTMS,

a 3D heat transfer model of the battery cells and coolant was established. The heat diffusion equation in battery cells can be expressed as follows

$$\rho c_{LIB} \frac{\partial T}{\partial t} = \nabla \cdot (k \nabla T) + \dot{q}''' \tag{6}$$

where ρ is the average density of the battery cell, k is the effective heat conductivity, and $\dot{q}'''$ is the volumetric heat generation rate of the battery. The effective thermal conductivity of the cell depends on its direction, and it equals to 1.2 W/(m·K) in the radial direction and 34.4 W/(m·K) in the axial direction. The volumetric heat source $\dot{q}'''$ is determined by the polynomial fitting equation from the experimental data based on Eq. (5).

For the coolant, such as dielectric liquid and air, the mass continuity equation, the momentum conservation equation, and the energy conservation equation are given by [60]

$$\frac{\partial \rho_c}{\partial t} + \nabla \cdot (\rho_c \vec{v}) = 0 \tag{7}$$

$$\frac{\partial (\rho_c \vec{v})}{\partial t} + \nabla \cdot (\rho_c \vec{v} \vec{v}) = -\nabla p + \nabla \cdot (\mu_c \vec{v}) \tag{8}$$

$$\frac{\partial (\rho_c c_{pc} T_c)}{\partial t} + \nabla \cdot (\rho_c c_{pc} T_c \vec{v}) = \nabla \cdot (k_c \nabla T_c) \tag{9}$$

where ρ_c is the coolant density, $\vec{v}$ is the coolant velocity vector, μ_c is the dynamic viscosity of the coolant, and c_{pc} is the specific heat of the coolant.

For the immersion liquid and the battery module, the thermo-physical parameters were selected from Tables 1 and 2. The conductivity of the engineering fluid was taken as 0.6 W/(m·K) adjusted by experiments which agrees with the previous study [61]. The thermal properties of air at 25 °C were obtained using the polynomial functions in COMSOL. The temperature-dependent thermal properties of air were depicted in Fig. S3, and the polynomial functions were summarized in Table S1.

3.3. Boundary conditions and mesh sensitivity analysis

The initial temperature values of the cell and coolants (air and immersion liquid) were set at 25 °C, which was commonly used by previous studies [62]. For the forced air-cooling case, the boundary condition for the inlet airflow rate was 0.35 m/s, and the boundary condition for the outlet was the pressure out, which was set as the standard atmospheric pressure. In the immersion cooling case, the constant temperature of 22 °C was selected for the outside boundary condition to simulate the experimental tests. As the Reynolds numbers for coolants are less than 2300, the laminar model was employed for the numerical simulation.

The gravity of the cooling liquid was also considered. The heat generation rate of heating sources (i.e., battery cells) was set as the 5th polynomial function based on Eq. (4). The no-slip boundary condition was adopted between cells and the coolants for all investigated cases. To simplify the simulation, the thermal resistance of the acrylic box was ignored in this study. A transient thermal model

was utilized to simulate the temperature variation of the batteries under different working conditions.

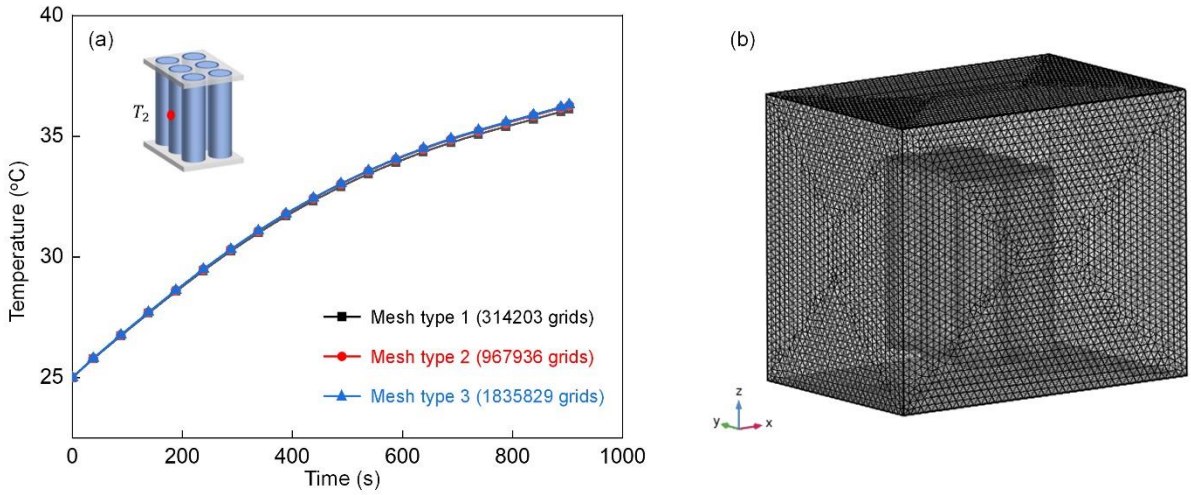

Fig. 4. (a) The predicted temperature evolutions of cell-2 (T_2) with different gird resolutions during the 3C discharge, and (b) the finite element model for the selected meshing strategy.

The numerical model was solved by the commercial software COMSOL Multiphysics 5.6. Free tetrahedron mesh was selected for the cells and coolants. To ensure the accuracy of simulation results, the sensitivity analysis of mesh was conducted. As illustrated in Fig. 4a, the temperature evolution of cell-2 (T_2) during 3C discharge was summarized from three numerical cases with grid numbers of 314,203, 967,936, and 1,835,829. Apparently, the differences between these three temperature responses were relatively small. Hence, the grid structure involving 967,936 elements was used in this work (Fig. 4b), which can save computation time and provide adequate accuracy. The selected grid structure has an average element quality of 0.66.

4. Results and discussion

4.1. Typical battery thermal performance under air cooling

Comparing the thermal management performance of different cooling strategies is one of the significant purposes of this work. Taking a cycling rate of 3C as an example, Fig. 5 plots the experimental data of module voltage, cell temperature, and the maximum temperature difference varying with time for the conventional air-cooling condition. The module voltage can assist in distinguishing the stage of the cycling test, while the cell temperature and maximum temperature difference can help to assess the thermal management performance. The maximum temperature difference (ΔT) is calculated by [52]

$$\Delta T(t) = max\{T_i(t)\} - min\{T_i(t)\}, i \in \{1, 2, 3, 4, 5, 6\} \quad (10)$$

where t denotes the cycling time, and the i stands for the cell number, i.e., 1, 2, 3, 4, 5, and 6.

As shown in Fig. 5a, the module is in the CC-CV charging mode at the beginning. It can be

observed that the cell temperature first increases and then decreases during the charging process. The temperature increase is mainly attributed to the Joule heat induced by internal resistance overcoming the endothermic reactions during the CC charging stage. As the charging mode is changed from CC to CV, the charging current decreases. This leads to a lower joule heat generation, so the temperature falls during the CV mode. After the rest, the battery module starts to discharge with a constant current of 3C. During the discharging period, the battery temperature significantly increases due to the Joule heat and internal exothermic reactions.

Even though the generated Joule heat could be the same for the charging and discharging processes, different reaction modes of endothermic and exothermic contribute to a higher temperature increase for the discharging process, agreeing with the previous studies [52]. Moreover, the charging could also be affected by the thickness ratio of the current collector to the active layer [63]. Plastic strain can cause the active layer to fracture and become detached from the current collector, which might accelerate battery aging [64,65]. Therefore, the maximum cell temperature (T_{max}) during discharging was employed in considerable studies to evaluate the performance of BTMS. For the natural cooling condition in Fig. 5a, the value of T_{max} is around 69 °C, which is much higher than the optimal operating temperature range for batteries (20 ~ 40 °C). Additionally, the maximum value for ΔT during the entire cycling process is 6.9 °C, exceeding the suggested temperature difference of 5 °C.

Fig. 5b shows the historical experimental data for the forced air-cooling system at 3C cycling. The tendency for temperature evolution is similar to natural cooling. The value of T_{max} under forced air cooling is 48 °C, which is still higher than the ideal temperature range despite being 21 °C lower than natural cooling. Similarly, the highest value for ΔT is 6.2 °C, which is slightly greater than the ideal temperature gradient inside the battery module (5 °C). Therefore, forced air-cooling can reduce the maximum battery temperature while temperature homogeneity still needs to be facilitated.

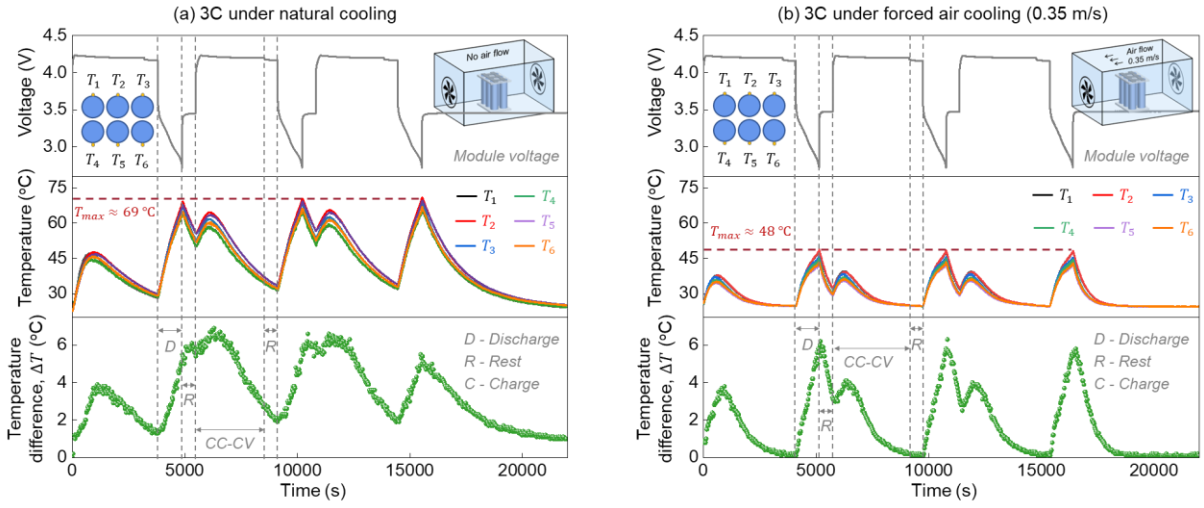

Fig. 5. Variation curves of module voltage, cell temperature, and temperature difference (ΔT) for 3C cycling under (a) natural convection and (b) forced air cooling.

4.2. Battery thermal performance under liquid immersion cooling

With the aid of liquid immersion cooling, the electro-thermal characteristics of battery modules at 3C cycling are summarized in this section. In Fig. 6a, the maximum temperature of cells (T_{max}) is 37 °C, reduced by 46% compared to the natural cooling condition. The maximum ΔT is 1.8 °C, which is much lower than that of conventional air cooling. In short, both the T_{max} and ΔT in the immersion cooling system can satisfy the optimal temperature range and healthy temperature gradient. However, the initial cell temperature and maximum cell temperature (T_{max}) during discharge seems to elevate slightly with the number of cycles. This could be caused by two reasons: (1) the resting time after each cycle is too short for cells to drop their temperature to the initial value; and (2) the temperature of the static liquid coolant could also have increased slightly during the discharging process, affecting its cooling efficiency.

To figure out the influence of these two factors, one more charge-discharge cycle with different initial voltage was conducted in Fig. 6b. Obviously, the T_{max} of the first three discharging processes slightly increases with the cycling number, while it does not rise after the third cycle. Therefore, static immersion cooling can maintain the maximum battery temperature below 40 °C and a maximum temperature difference lower than 5 °C at a high cycling rate of 3C, indicating an excellent performance of battery thermal management.

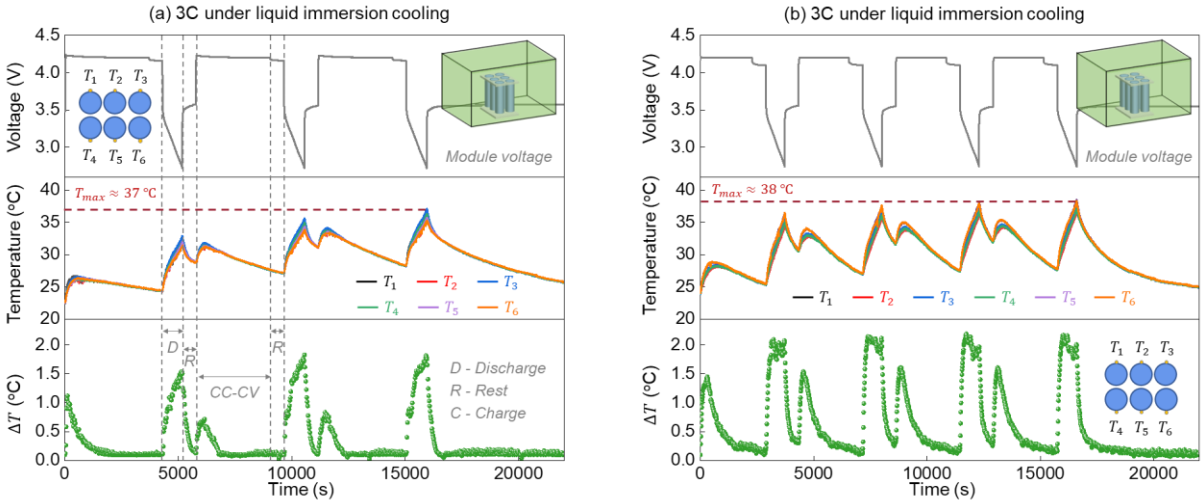

Fig. 6. Variation curves of module voltage, cell temperature, and temperature difference (ΔT) for immersion cooling system at 3C cycling with (a) 3 discharge stages and (b) 4 discharge stages.

4.3. Comparison between immersion cooling and conventional air cooling

The above values of T_{max} are from multiple discharging processes with various initial cell temperatures of 25 ± 5 °C. To compare the thermal management performance directly, Fig. 7 extracted the temperature variation curves from the repeating discharge tests with an equal initial temperature of 25 ± 0.5 °C. For different cooling strategies, two repeat cases were selected, and the average cell temperature varying with time was depicted. As shown in Fig. 7, the average surface temperature for cells displays an increasing trend with time. As expected, the cooling performance ranks as follows:

liquid immersion cooling > forced air cooling > natural cooling. For 1C discharge cases in Fig. 7a, the maximum cell temperatures under three different cooling strategies are below 40 °C, within the optimal temperature range. At a higher discharge rate of 3C, cell temperature increases and exceeds 40 °C under natural cooling and forced air cooling (Fig. 7b). Only immersion cooling can maintain the cell temperature within the safety region (20 ~ 40 °C) at 3C discharge. The above result suggests that immersion cooling can substantially reduce the maximum cell temperature during the discharging process.

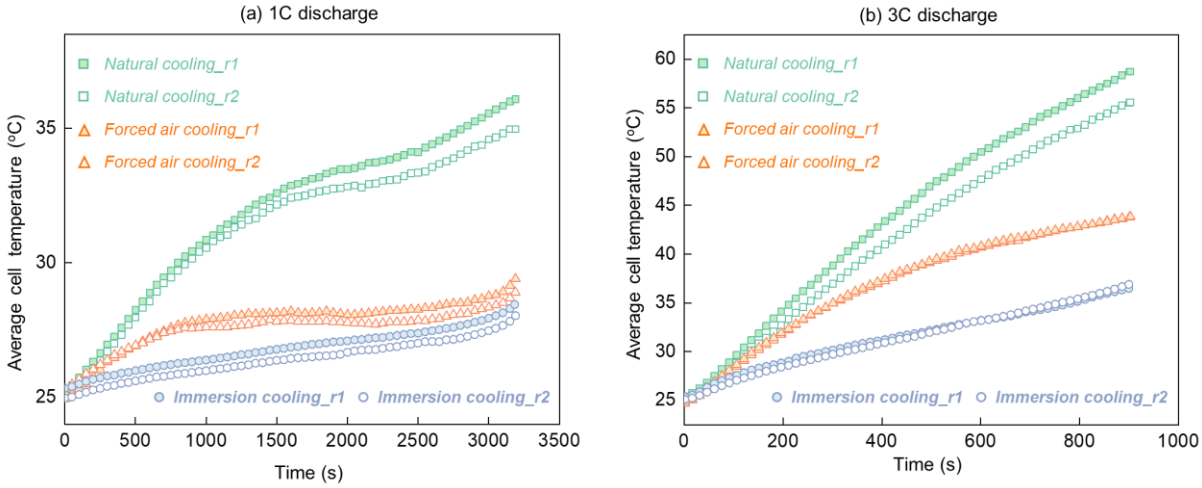

Fig. 7. The average temperature variations for cells under (a) 1C discharge and (b) 3C discharge, where "r1" and "r2" represent the first and second repeated experiments.

For a more straightforward comparison, the maximum cell temperature (T_{max}) and the maximum temperature difference (ΔT_{max}) for the extracted repeating test are summarized in Fig. 8. The initial cell temperature is around 25 ± 0.5 °C. As demonstrated in Fig. 8a, the measured maximum temperature (T_{max}) increases with C-rate, agreeing with the previous studies. Specifically, the value of T_{max} increases from 36.8 °C to 59.6 °C as the discharge rate increases from 1C to 3C under the natural cooling condition. More importantly, as the cooling strategies change from natural cooling to immersion cooling, the decrements of T_{max} are around 22%, 39%, and 39% during the 1C, 2C, and 3C discharging processes, respectively.

As for temperature uniformity, Fig. 8b shows the maximum temperature difference (ΔT_{max}) varying with the C-rate. Similarly, the value of ΔT_{max} increases with the C-rate for all cooling methods. Moreover, the immersion cooling system has the lowest value of ΔT_{max} which is lower than 3 °C at all C-rates. Therefore, the proposed immersion cooling method exhibits excellent cooling performance for battery thermal management. The following sections will numerically analyze the cooling capacity of the proposed immersion cooling method and further optimize it for the actual application.

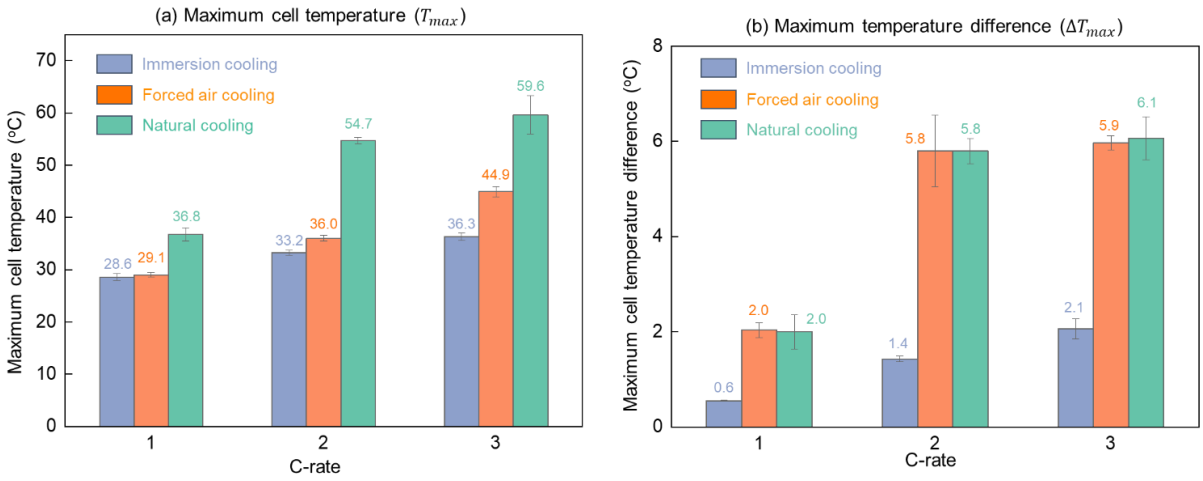

Fig. 8. The measured (a) maximum cell temperature (T_{max}) and (b) maximum temperature difference (ΔT_{max}) for the battery module during discharge, where the initial cell temperature is 25 ± 0.5 °C.

4.4. Model validation and energy flow analysis

As discussed above, the value of T_{max} and ΔT_{max} increases with C-rate. Hence, the numerical simulation of this work focuses on the scenario with a high discharge rate of 3C. Fig. 9 compares the experimental data measured by thermocouples with simulated results for both forced air cooling and immersion cooling systems. The temperature evolution at the mid-height surface cell-2 (T_2) is selected for model validation (the same position in Fig. 4). Obviously, the experimental and numerical results agree well with each other, with an average error of 2.9% and 2.2% for immersion cooling and forced air cooling systems. Therefore, it is confirmed that the numerical model can deliver accurate results.

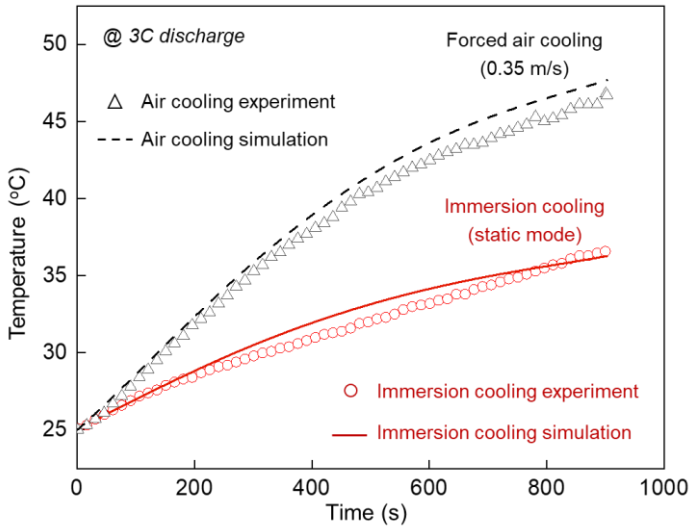

Fig. 9. Comparison of measured and simulated temperature data during 3C discharge.

Fig. 10 further compares the temperature distribution of cells and coolants during the 3C discharging process. With forced air cooling, there is a significant temperature gradient within the battery system. Cells near the air outlet are much hotter than cells near the air inlet. Particularly, cell-2

has the highest temperature, which is consistent with the experimental results. With immersion cooling, the battery system displays a lower and more uniform temperature profile. By calculating the average volume temperature of different cells, curves for maximum temperature difference are seen in Fig. 10c.

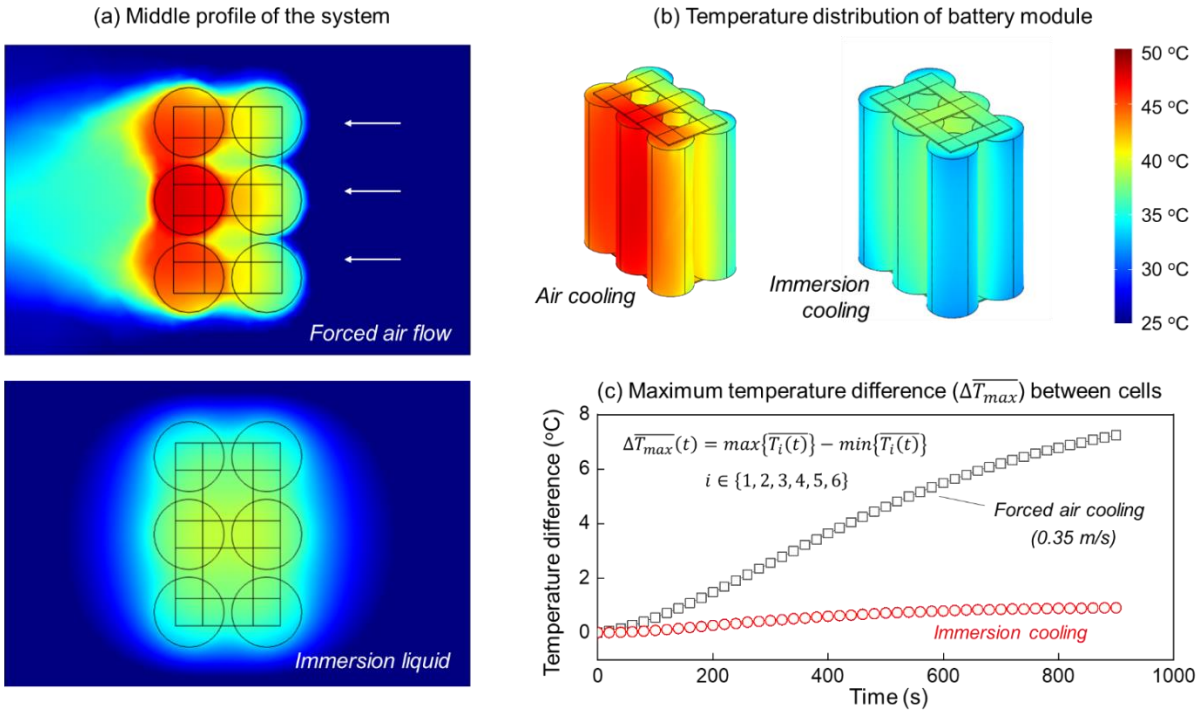

Fig. 10. Temperature distributions for (a) mid-profile of the entire cooling systems and (b) battery module at the end of 3C discharge, as well as (c) the evolution curves of maximum cell temperature difference.

As expected, immersion cooling allows for a more even temperature distribution, which can benefit the performance of the battery system. Moreover, the value of the maximum temperature difference for immersion cooling is much lower than the experimental results in Fig. 8b. The reason should be that the experiments measure the point temperature of the cell surface, whereas the numerical model considers the entire volume temperature. Therefore, in the following sections, the numerical results will be used to quantitatively analyze the efficiency of the immersion cooling strategy.

As it is difficult to measure the liquid temperature gradient during the experiments, the numerical results are utilized to quantitatively compare the cooling performance for the air cooling and liquid immersion cooling. The effective cooling rate ($\dot{q}_c$) and the total amount of dissipated heat (Q_c) are set as the comparison criterion. The transient cooling rate ($\dot{q}_c$) is calculated from the heat flux ($\dot{q}_c''$) from cells to the coolants (i.e., air and immersion liquid) through the COMSOL software as

$$\dot{q}_c(t) = \dot{q}_c''(t)A \tag{11}$$

where A is the surface area of the cell. Then, the equivalent energy of heat dissipation (Q_c) is given by

$$Q_c(t) = \int_0^t \dot{q}_c(t)dt \tag{12}$$

where t denotes the discharge time. Taking cell-2 which has the poorest cooling condition under air cooling as an example, Fig. 11 shows the values of $\dot{q}_c$ and Q_c varying with time (t) during the 3C discharge. It is clear that both the values of $\dot{q}_c$ and Q_c increase with time and reach the maximum value at the end of 3C discharge.

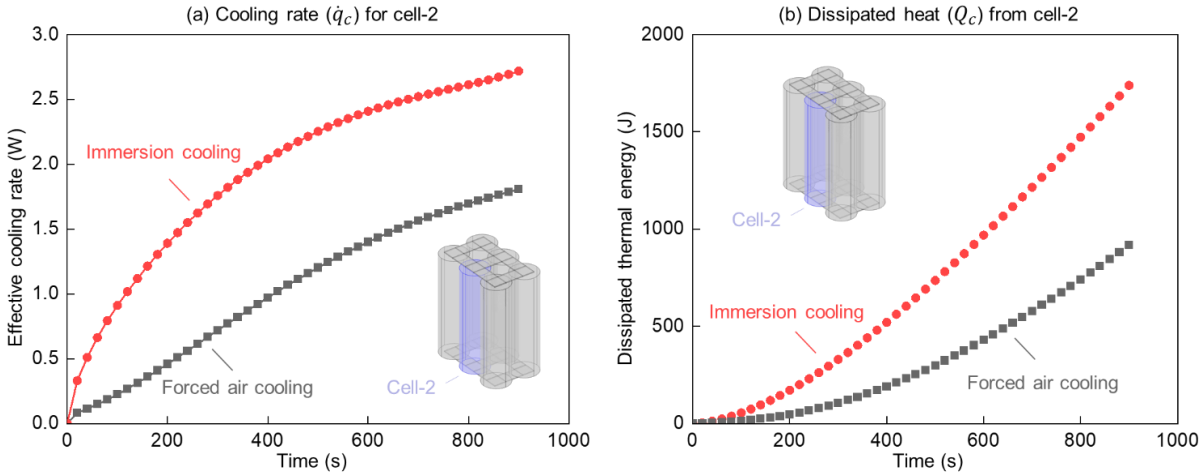

Fig. 11. (a) Effective cooling rate for different cooling strategies and (b) overall cooling for cell-2 at 3C discharge.

Fig. 11a suggests that the immersion-cooling rate is much higher than the air-cooling rate. The average value of $\dot{q}_c$ for immersion cooling is about 2.5 times higher than the air cooling during the 3C discharge. However, the ratio between them decreases to 1.5 times at the end of 3C discharge. Specifically, the final values for immersion cooling and air-cooling rates are 2.7 W and 1.8 W, respectively. This is because the temperature of the static liquid will increase during the discharge, which will reduce the increasing rate of $\dot{q}_c$ with time.

Nevertheless, the cooling capacity of immersion cooling is still enough to control the maximum battery temperature and cell temperature difference within an acceptable range. Totally, immersion cooling can remove the heat of 1,738 J from the battery at 3C discharge, accounting for 22% of the discharged electric energy (Fig. 11b). The dissipated heat is 90% greater than air cooling and is comparable to oil-based immersion cooling [52]. Therefore, both the experimental results and numerical analysis suggest that the static immersion cooling system proposed by this work can exhibit a wonderful capability for battery thermal management, even at 3C.

4.5. Modification of the simulated model for the actual application

During the experiments, a water tank was used to ensure the constant temperature of the acrylic box for the immersion cooling system and improve the experimental repeatability. Thus, the constant temperature boundary was considered for the above immersion cooling model. However, thermal convection would exist on the external wall of the immersion cooling system in the real application scenario. To provide valuable guidelines for practical applications, the numerical model was modified

and employed a free convection boundary condition on the external walls of the immersion cooling system. Referring to the linear fitting of Eq. (3) and literature data [60], a convective heat transfer coefficient of 5 W/(m^2·K) was selected.

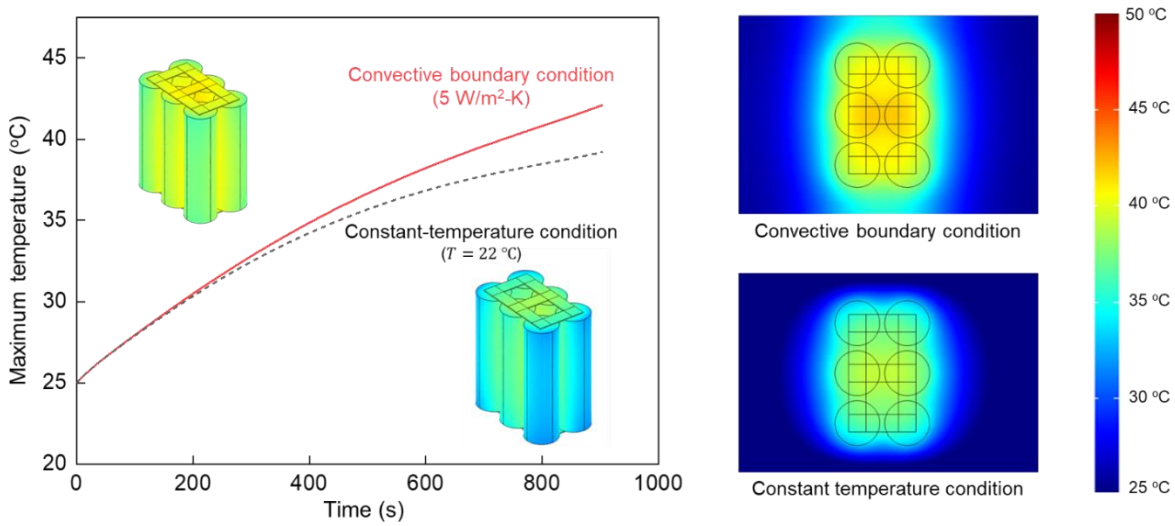

Fig. 12. Maximum temperature evolution for simulated cases with different boundary conditions, as well as the temperature distribution at the end of 3C discharge.

Fig. 12 shows the evolution of maximum temperature in the simulated model with different boundary conditions. The solid red line represents the modified case with a convective boundary condition, while the black dashed line indicates the model with constant temperature for the boundary condition. As expected, the maximum temperature of the modified model is a little bit higher than that of the original model. Specifically, the maximum temperature at the end of 3C discharge is 42 °C, which is 3 °C higher than the maximum temperature in the original model. Moreover, the temperature difference between cells in the modified model is still lower than 5 °C. In short, the maximum temperature for the modified case slightly exceeds the optimal temperature range, while the temperature discrepancy is below the threshold.

4.6. Influences of the liquid volume and ambient temperature for immersion cooling

To optimize the static immersion cooling system for battery thermal management applications, the effects of liquid volume and ambient temperature on cooling performance are further investigated at 3C discharge. Taking the battery module with 2-mm cell spacing as a baseline, we proportional enlarge the volume of the entire system and calculate the volume ratio of liquid to the battery module (δ). The selected battery/liquid volume ratio (δ) and the corresponding system dimensions are listed in Table 4.

Except for the liquid volume, the influence of ambient temperature on cooling performance is also studied in this work. In literature, the commonly used ambient temperatures for single-cell immersion cooling system is 15 °C ~ 30 °C [52]. Therefore, four ambient temperatures of 15 °C, 20 °C, 25 °C, and 30 °C are adopted to study the influences of ambient temperature (T_a) and the liquid-battery volume ratio (δ) on cooling performance at 3C discharge numerically.

Table 4. The studied liquid-battery volume ratio (δ) for a 6-cell battery module with a volume of 99 mL.

Case No.	I	II	III	IV
liquid-battery volume ratio, δ (-)	0.81	2.13	5.11	13.50
System dimension (mm)	42×62×69	50.4×74.4×82.8	63×93×103.5	84×124×138
Liquid volume (mL)	80.48	211.29	507.21	1338.22

At the ambient temperature of 20 °C, Fig. 13a describes the effect of the liquid volume on transient maximum temperature, i.e., $T_{max}(t)$ at 3C discharge. As expected, the system with a high value of δ shows a better cooling performance. Except for Case-I ($\delta = 0.81$) and Case-II ($\delta = 2.13$), all cases can control the maximum cell temperature below the safety threshold of 40 °C, indicating that increasing liquid volume can improve the cooling performance of the system. It should be noted that this improvement effect gradually attenuates for larger liquid volume ratios. Specifically, the decrement of the final maximum temperature is 14%, as δ increases from 0.81 to 2.13. However, the decrement of the final maximum temperature is only 2.4%, as δ increases from 5.11 to 13.5. Therefore, reducing the ambient temperature could be a more effective way to enhance the cooling performance.

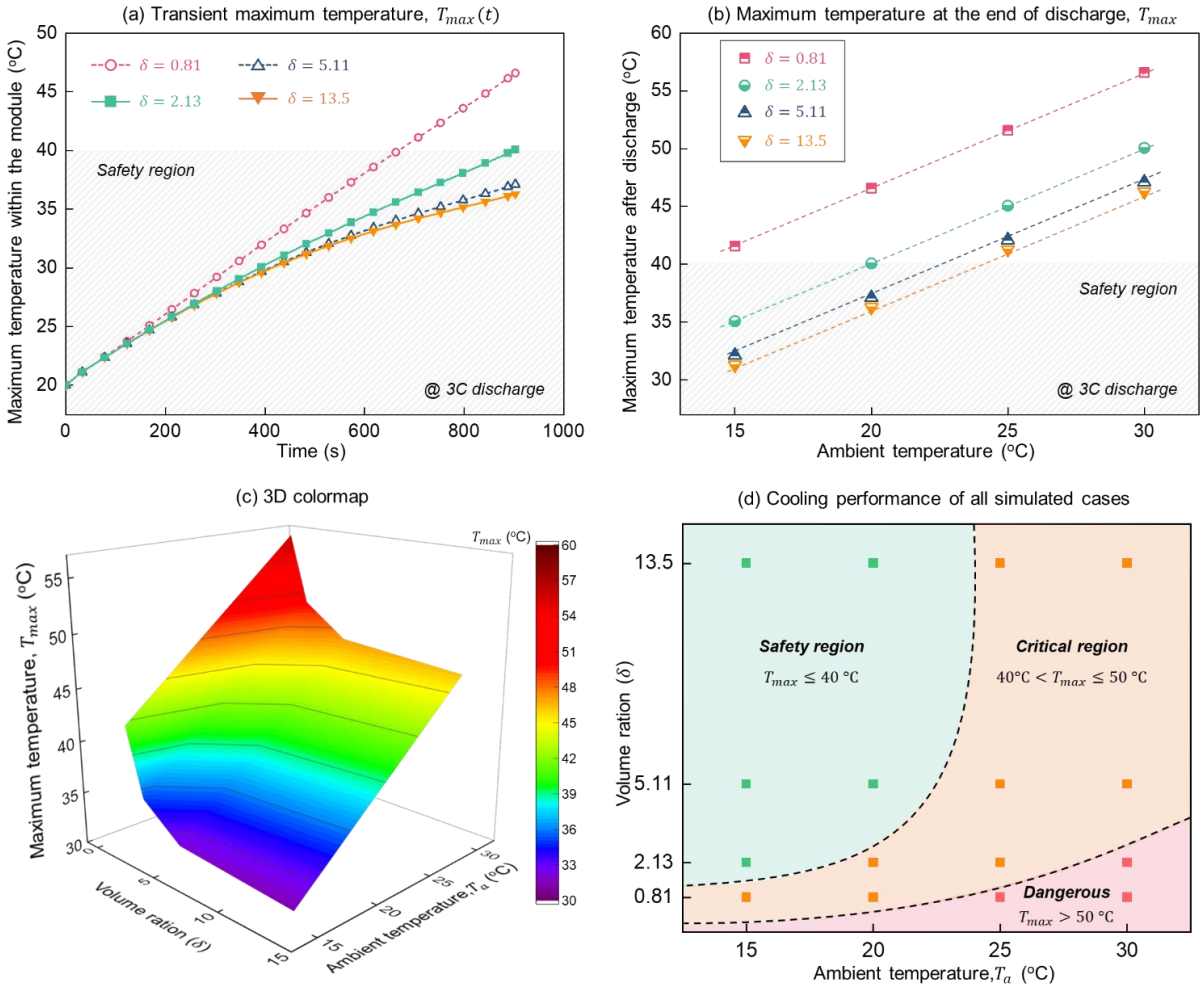

Fig. 13. (a) Evolution of transient maximum temperature for different cases at an ambient temperature of 20 °C, (b) the maximum temperatures of all cases at the end of 3C discharge, (c) 3D colormap indicating comprehensive effects of volume ratio and ambient temperature, and (d) region division for system

optimization.

Fig. 13b summarizes the maximum temperature of all simulated cases at the end of discharge. This terminal temperature (T_{max}) increases with ambient temperature but decreases with the liquid volume ratio. For Case-I ($\delta = 0.81$), the terminal temperature increases from 41.6 °C to 56.6 °C with an increment of 36% as the ambient temperature rises from 15 °C to 30 °C. In the meantime, such a terminal temperature is reduced by 25% as the liquid volume ratio rises to 13.5. In other words, the cooling performance of the proposed immersion cooling system would be enhanced at lower ambient temperature and larger liquid volume, and the influence of ambient temperature exceeds that of liquid volume.

Fig. 13c is the 3D colormap that illustrates the influences of liquid volume and ambient temperature on terminal maximum temperature. The color changes from purple to crimson as the corresponding maximum temperature increases from 30 °C to 60 °C. The system with different combinations of ambient temperature and volume ratio can lead to different terminal maximum temperatures. A lower ambient and larger liquid volume can achieve a lower maximum temperature, indicating a better cooling performance. The color map can be divided into three parts of maximum temperature lower than 40 °C, maximum temperature between 40 °C ~ 50 °C, and maximum temperature higher than 50 °C. Towards the parameter optimization for practical application, we define three regions of safety ($T_{max} \leq 40\ °C$), critical ($40\ °C < T_{max} \leq 50\ °C$), and dangerous ($T_{max} > 50\ °C$). Based on the criterion, the division of regions is presented in Fig. 13d. With the increase in ambient temperature, the lower limit of the safety region increases, leading to the decrease of its range dimension. Thus, the proposed immersion cooling system could be optimized by selecting the proper ambient temperature.

It should be noted that the critical region is also acceptable in the actual application [66]. For example, when the ambient temperature is lower than 25 °C, the system with a volume ratio (δ) higher than one is enough to control the maximum temperature to an ideal value. When the ambient temperature rises to 30 °C, the liquid volume should be at least two times larger than the battery module volume to achieve good thermal management. For electric vehicles, the driving conditions are relatively complex, and an ambient temperature higher than 25 °C should be a common condition. Given that a large volume ratio (δ) would sacrifice the energy density of the system, the flow-based immersion cooling is a good choice and will be investigated in future. Therefore, the static immersion cooling studied in this work is more suitable to be applied in the battery energy storage system where the ambient temperature can be easily controlled by the air condition system.

Considering the energy density of the entire system and thermal management performance, a volume ratio ranging from 0.8 to 2 and an ambient temperature ranging from 15 °C to 20 °C are recommended for the proposed immersion cooling system. The division of three regions could be adapted to other immersion cooling systems, where the threshold of each region depends on system

properties.

4.7. Effect of different coolants and the application on the large battery module

At an ambient temperature of 15 °C, the immersion-cooling BTMS with a volume ratio (δ) of 0.81 can restrict the maximum battery temperature below 42 °C, which is acceptable for the actual application [66]. In literature, other coolants like mineral oil and AmpCool AC-100 engineering fluid have been applied to the forced-flow immersion cooling system [49]. To explore the efficacy of these coolants on static-mode system, this section employed them to cool down the 6-cell and 100-cell battery module under 3C discharge. The thermal properties of these two coolants are presented in Table 5.

Table 5. Properties of mineral oil and AC-100 fluid used for simulation [49].

Coolants	Density [kg/m^3]	Dynamic viscosity [Pa·s]	Specific heat [J/kg·K]	Thermal conductivity [W/(m·K)]
Mineral oil	924	0.05	1900	0.13
AC-100	811	0.008	2203.2	0.1373

Fig. 14a demonstrates the effect of different coolants on the transient maximum temperature of the 6-cell battery module under 3C discharge. The volume ratio (δ) is chosen as 0.81, and the ambient temperature is 15 °C. At the end of 3C discharge, the maximum temperature values in different immersion cooling systems are around 42°C. The similar cooling performance of mineral oil and AC-100 engineering fluid is consistent with the research results reported by Jithin and Rajesh [49]. This further verifies the reliability of the numerical model proposed in this work. The static immersion cooling method is then applied to a 100-cell module (Fig. 14b).

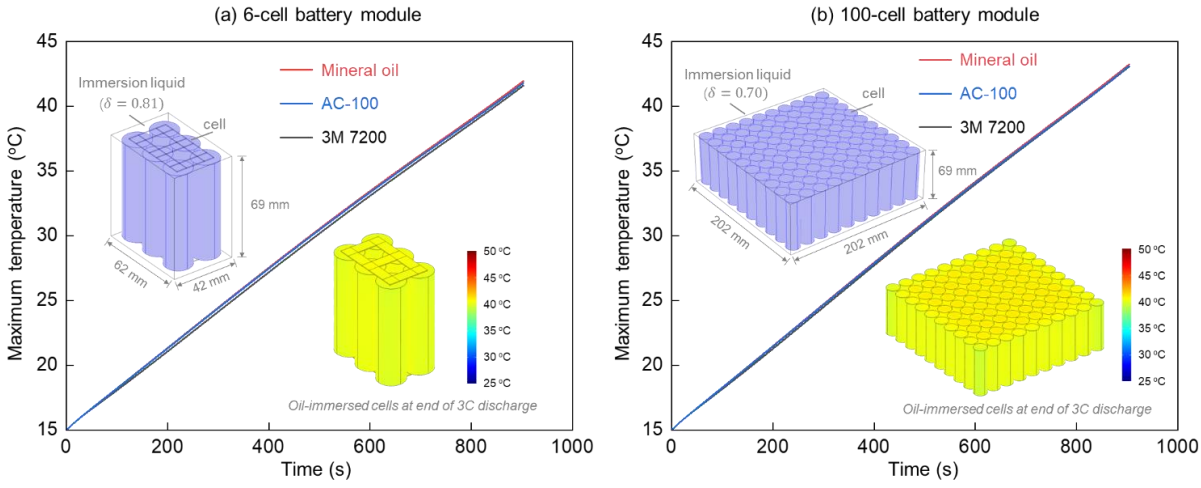

Fig. 14. Comparison of different coolants for the (a) 6-cell battery module with a liquid-battery volume ratio of 0.81 and (b) 100-cell battery module with a liquid-battery volume ratio of 0.7.

To simplify the problem and save the computational cost, the tabs are ignored. As shown in Fig. 14b, the dimensions of the immersion cooling domain are 120 mm × 80 mm × 100 mm, with a liquid-

battery volume ratio (δ) of 0.7. Although the maximum temperature in Fig. 14b is a little bit higher due to the lower δ, all three coolants are able to keep the cell temperature below 45 °C. Therefore, the proposed static immersion cooling method has great potential for use in large-scale battery systems.

Recently, the world's first immersion-cooled energy storage station was launched in Guangdong, China [67]. It is the largest grid-side independent power storage plant in southern China, where forced-flow immersion cooling is employed to control the temperature of prismatic cells. Towards a safe and low energy consumption future, cylindrical cells with natural immersion cooling would be another promising energy storage solution. As cylindrical cell has a large surface-volume ratio, the efficiency of immersion cooling would be superior [52]. From the fundamental aspect of heat transfer, this work confirms that natural immersion cooling can meet the stringent thermal management requirements of large-scale cylindrical battery modules. Overall, the immersion cooling strategy has the potential for massive application in battery energy storage systems, which requires more fundamental research.

5. Conclusions

This work compares the cooling performance between the immersion cooling system and conventional air-cooling systems at different C-rates. Results indicate that the maximum cell temperature (T_{max}) appears at the end of discharge, which increases with the C-rate. The value of T_{max} under natural cooling at the 3C discharge can exceed 60 °C at room temperature, threatening battery safety. Employing the forced air-cooling with an airflow rate of 0.35 m/s, the maximum cell temperature would decrease to 44.9 °C at the end of 3C discharge, but the cell temperature difference is still higher than 6 °C. The proposed static immersion cooling system exhibits an excellent cooling capability that controls the maximum cell temperature below 40 °C and cell temperature gradient within 3 °C during 3C cycling tests.

3D numerical results suggest that the immersion cooling method has a maximum cooling rate of 2.7 W for the cell with the highest temperature, 50% higher than the forced air-cooling system. Towards the practical application, the numerical models were modified to investigate the effects of ambient temperature and liquid-battery volume on system cooling efficiency. It is confirmed that cooling performance would be enhanced at lower ambient temperature and larger liquid volume, and the influence of ambient temperature exceeds that of liquid volume.

From the perspective of system energy density and thermal safety, the liquid-to-battery volume ratio of 0.8 ~ 2 and the ambient temperature of 15 ~ 20 °C are recommended for the proposed immersion cooling system. Then, different cooling regions are defined to evaluate the thermal-management performance and help optimize the immersion cooling system. Finally, the cooling efficiency of other fluids (mineral oil and AC-100 engineering fluid) in the 100-cell battery modules further verifies the feasibility of the proposed immersion cooling methods for large-scale battery systems. These results can provide useful information and scientific guidelines for battery thermal management to ensure safe operation of battery energy storage systems.

CRediT authorship contribution statement

Yanhui Liu: Data curation, Investigation, Writing - Original Draft, Formal analysis. **Gulzhan Aldan:** Data curation, Investigation, Resourcing, Writing - Review & Editing. **Xinyan Huang:** Conceptualization, Methodology, Funding acquisition, Supervision, Writing - Review & Editing. **Menglong Hao:** Methodology, Formal analysis, Supervision.

Acknowledgments

This work is kindly supported by the National Key R&D Program of China (2022YFE0207400), Early Career Scheme of Hong Kong Research Grant Council (25205519), and Shenzhen Science and Technology Program (JCYJ20210324131006017).

References

[1] Offer G, Patel Y, Hales A, Bravo Diaz L, Marzook M. Cool metric for lithium-ion batteries could spur progress. *Nature* 2020;582:485–7.

[2] Hao M, Li J, Park S, Moura S, Dames C. Efficient thermal management of Li-ion batteries with a passive interfacial thermal regulator based on a shape memory alloy. *Nature Energy* 2018;3:899–906.

[3] Lin J, Liu X, Li S, Zhang C, Yang S. A review on recent progress, challenges and perspective of battery thermal management system. *International Journal of Heat and Mass Transfer* 2021;167:120834.

[4] Zeng Y, Chalise D, Lubner SD, Kaur S, Prasher RS. A review of thermal physics and management inside lithium-ion batteries for high energy density and fast charging. *Energy Storage Materials* 2021;41:264–88.

[5] Liu Y, Niu H, Xu C, Huang X. Thermal runaway propagation in linear battery module under low atmospheric pressure. *Applied Thermal Engineering* 2022;216:119086.

[6] Niu H, Chen C, Ji D, Li L, Li Z, Liu Y, et al. Thermal-Runaway Propagation over a Linear Cylindrical Battery Module. *Fire Technology* 2020;56:2491–507.

[7] Liu H, Wei Z, He W, Zhao J. Thermal issues about Li-ion batteries and recent progress in battery thermal management systems: A review. *Energy Conversion and Management* 2017;150:304–30.

[8] Roe C, Feng X, White G, Li R, Wang H, Rui X, et al. Immersion cooling for lithium-ion batteries – A review. *Journal of Power Sources* 2022;525:231094.

[9] Wu W, Wang S, Wu W, Chen K, Hong S, Lai Y. A critical review of battery thermal performance and liquid based battery thermal management. *Energy Conversion and Management* 2019;182:262–81.

[10] Xie Y, Liu Y, Fowler M, Tran M, Panchal S, Li W, et al. Enhanced optimization algorithm for the structural design of an air-cooled battery pack considering battery lifespan and consistency. *International Journal of Energy Research* 2022;46:24021–44.

[11] Khaboshan HN, Jaliliantabar F, Abdullah AA, Panchal S. Improving the cooling performance of cylindrical lithium-ion battery using three passive methods in a battery thermal management system. *Applied Thermal Engineering* 2023;227:120320.

[12] Talele V, Patil MS, Panchal S, Fraser R, Fowler M, Gunti SR. Novel metallic separator coupled composite phase change material passive thermal design for large format prismatic battery pack. *Journal of Energy Storage* 2023;58:106336.

[13] Li W, Xie Y, Hu X, Tran M-K, Fowler M, Panchal S, et al. An internal heating strategy for lithium-ion batteries without lithium plating based on self-adaptive alternating current pulse. *IEEE Transactions on*

Vehicular Technology 2022.

[14] Panchal S, Pierre V, Cancian M, Gross O, Estefanous F, Badawy T. Development and Validation of Cycle and Calendar Aging Model for 144Ah NMC/Graphite Battery at Multi Temperatures, DODs, and C-Rates. SAE Technical Paper; 2023.

[15] Braga R, Mevawalla A, Gudiyella S, Panchal S, Giuliano M, Nicol G, et al. Transient Electrochemical Modeling and Performance Investigation Under Different Driving Conditions for 144Ah Li-ion Cell with Two Jelly Rolls. SAE Technical Paper; 2023.

[16] Choudhari V, Dhoble AS, Panchal S, Fowler D, Fraser D. Experimental and Numerical Investigation on Thermal Characteristics of 2× 3 Designed Battery Module. *Available at SSRN* n.d.

[17] Zhao G, Wang X, Negnevitsky M, Zhang H. A review of air-cooling battery thermal management systems for electric and hybrid electric vehicles. *Journal of Power Sources* 2021;501:230001.

[18] Liu Y, Sun P, Lin S, Niu H, Huang X. Self-heating ignition of open-circuit cylindrical Li-ion battery pile: Towards fire-safe storage and transport. *Journal of Energy Storage* 2020;32:101842.

[19] Sun P, Bisschop R, Niu H, Huang X. A Review of Battery Fires in Electric Vehicles. *Fire Technology* 2020;56:1361–410.

[20] Lee S, Han U, Lee H. Development of a hybrid battery thermal management system coupled with phase change material under fast charging conditions. *Energy Conversion and Management* 2022;268:116015.

[21] Feng R, Huang P, Tang Z, He Y, Bai Z. Experimental and numerical study on the cooling performance of heat pipe assisted composite phase change material-based battery thermal management system. *Energy Conversion and Management* 2022;272:116359.

[22] Ahmad S, Liu Y, Khan SA, Hao M, Huang X. Hybrid battery thermal management by coupling fin intensified phase change material with air cooling. *Journal of Energy Storage* 2023;64:107167.

[23] Weng J, Huang Q, Li X, Zhang G, Ouyang D, Chen M, et al. Safety issue on PCM-based battery thermal management: Material thermal stability and system hazard mitigation. *Energy Storage Materials* 2022;53:580–612.

[24] Zhou H, Dai C, Liu Y, Fu X, Du Y. Experimental investigation of battery thermal management and safety with heat pipe and immersion phase change liquid. *Journal of Power Sources* 2020;473:228545.

[25] Chitta SD, Akkaldevi C, Jaidi J, Panchal S, Fowler M, Fraser R. Comparison of lumped and 1D electrochemical models for prismatic 20Ah LiFePO4 battery sandwiched between minichannel cold-plates. *Applied Thermal Engineering* 2021;199:117586.

[26] Tang X, Guo Q, Li M, Wei C, Pan Z, Wang Y. Performance analysis on liquid-cooled battery thermal management for electric vehicles based on machine learning. *Journal of Power Sources* 2021;494:229727.

[27] Sheng L, Zhang H, Su L, Zhang Z, Zhang H, Li K, et al. Effect analysis on thermal profile management of a cylindrical lithium-ion battery utilizing a cellular liquid cooling jacket. *Energy* 2021;220:119725.

[28] Kong D, Peng R, Ping P, Du J, Chen G, Wen J. A novel battery thermal management system coupling with PCM and optimized controllable liquid cooling for different ambient temperatures. *Energy Conversion and Management* 2020;204:112280.

[29] Guo Z, Xu Q, Wang Y, Zhao T, Ni M. Battery thermal management system with heat pipe considering battery aging effect. *Energy* 2023;263:126116.

[30] Kim J, Oh J, Lee H. Review on battery thermal management system for electric vehicles. *Applied Thermal Engineering* 2019;149:192–212.

[31] Darcovich K, MacNeil DD, Recoskie S, Cadic Q, Ilinca F. Comparison of cooling plate configurations for

automotive battery pack thermal management. *Applied Thermal Engineering* 2019;155:185–95.

[32] Wang Y, Zhang G, Yang X. Optimization of liquid cooling technology for cylindrical power battery module. *Applied Thermal Engineering* 2019;162:114200.

[33] Deng Y, Feng C, E J, Zhu H, Chen J, Wen M, et al. Effects of different coolants and cooling strategies on the cooling performance of the power lithium ion battery system: A review. *Applied Thermal Engineering* 2018;142:10–29.

[34] Wu S, Lao L, Wu L, Liu L, Lin C, Zhang Q. Effect analysis on integration efficiency and safety performance of a battery thermal management system based on direct contact liquid cooling. *Applied Thermal Engineering* 2022;201:117788.

[35] Li X, Zhou Z, Zhang M, Zhang F, Zhou X. A liquid cooling technology based on fluorocarbons for lithium-ion battery thermal safety. *Journal of Loss Prevention in the Process Industries* 2022;78:104818.

[36] Suresh Patil M, Seo J-H, Lee M-Y. A novel dielectric fluid immersion cooling technology for Li-ion battery thermal management. *Energy Conversion and Management* 2021;229:113715.

[37] Zhou Y, Wang Z, Xie Z, Wang Y. Parametric Investigation on the Performance of a Battery Thermal Management System with Immersion Cooling. *Energies* 2022;15.

[38] Wang H, Tao T, Xu J, Shi H, Mei X, Gou P. Thermal performance of a liquid-immersed battery thermal management system for lithium-ion pouch batteries. *Journal of Energy Storage* 2022;46:103835.

[39] Sundin DW, Sponholtz S. Thermal Management of Li-Ion Batteries With Single-Phase Liquid Immersion Cooling. *IEEE Open Journal of Vehicular Technology* 2020;1:82–92.

[40] Le Q, Shi Q, Liu Q, Yao X, Ju X, Xu C. Numerical investigation on manifold immersion cooling scheme for lithium ion battery thermal management application. *International Journal of Heat and Mass Transfer* 2022;190:122750.

[41] Al Qubeissi M, Almshahy A, Mahmoud A, Al-Asadi MT, Raja Ahsan Shah RM. Modelling of battery thermal management: A new concept of cooling using fuel. *Fuel* 2022;310:122403.

[42] Chen D, Jiang J, Kim G-H, Yang C, Pesaran A. Comparison of different cooling methods for lithium ion battery cells. *Applied Thermal Engineering* 2016;94:846–54.

[43] Tan X, Lyu P, Fan Y, Rao J, Ouyang K. Numerical investigation of the direct liquid cooling of a fast-charging lithium-ion battery pack in hydrofluoroether. *Applied Thermal Engineering* 2021;196:117279.

[44] Al-Zareer M, Dincer I, Rosen MA. Novel thermal management system using boiling cooling for high-powered lithium-ion battery packs for hybrid electric vehicles. *Journal of Power Sources* 2017;363:291–303.

[45] van Gils RW, Danilov D, Notten PHL, Speetjens MFM, Nijmeijer H. Battery thermal management by boiling heat-transfer. *Energy Conversion and Management* 2014;79:9–17.

[46] Li Y, Zhou Z, Hu L, Bai M, Gao L, Li Y, et al. Experimental studies of liquid immersion cooling for 18650 lithium-ion battery under different discharging conditions. *Case Studies in Thermal Engineering* 2022;34:102034.

[47] Wang Y-F, Wu J-T. Thermal performance predictions for an HFE-7000 direct flow boiling cooled battery thermal management system for electric vehicles. *Energy Conversion and Management* 2020;207:112569.

[48] Trimbake A, Singh CP, Krishnan S. Mineral Oil Immersion Cooling of Lithium-Ion Batteries: An Experimental Investigation. *Journal of Electrochemical Energy Conversion and Storage* 2021;19.

[49] Jithin K V, Rajesh PK. Numerical analysis of single-phase liquid immersion cooling for lithium-ion battery thermal management using different dielectric fluids. *International Journal of Heat and Mass Transfer* 2022;188:122608.

[50] Liu J, Fan Y, Xie Q. Feasibility study of a novel oil-immersed battery cooling system: Experiments and theoretical analysis. *Applied Thermal Engineering* 2022;208:118251.

[51] Solai E, Guadagnini M, Beaugendre H, Daccord R, Congedo P. Validation of a data-driven fast numerical model to simulate the immersion cooling of a lithium-ion battery pack. *Energy* 2022;249:123633.

[52] Liu J, Fan Y, Wang J, Tao C, Chen M. A model-scale experimental and theoretical study on a mineral oil-immersed battery cooling system. *Renewable Energy* 2022;201:712–23.

[53] Liu Y, Niu H, Liu J, Huang X. Layer-to-layer thermal runaway propagation of open-circuit cylindrical li-ion batteries: Effect of ambient pressure. *Journal of Energy Storage* 2022;55:105709.

[54] Xie L, Huang Y, Lai H. Coupled prediction model of liquid-cooling based thermal management system for cylindrical lithium-ion module. *Applied Thermal Engineering* 2020;178:115599.

[55] Weng J, He Y, Ouyang D, Yang X, Chen M, Cui S, et al. Honeycomb-inspired design of a thermal management module and its mitigation effect on thermal runaway propagation. *Applied Thermal Engineering* 2021;195:117147.

[56] Lin X, Zhang X, Liu L, Yang M. Optimization Investigation on Air Phase Change Material Based Battery Thermal Management System. *Energy Technology* 2021;9:2100060.

[57] Zhao J, Rao Z, Huo Y, Liu X, Li Y. Thermal management of cylindrical power battery module for extending the life of new energy electric vehicles. *Applied Thermal Engineering* 2015;85:33–43.

[58] Fan Y, Bao Y, Ling C, Chu Y, Tan X, Yang S. Experimental study on the thermal management performance of air cooling for high energy density cylindrical lithium-ion batteries. *Applied Thermal Engineering* 2019;155:96–109.

[59] He CX, Yue QL, Wu MC, Chen Q, Zhao TS. A 3D electrochemical-thermal coupled model for electrochemical and thermal analysis of pouch-type lithium-ion batteries. *International Journal of Heat and Mass Transfer* 2021;181:121855.

[60] Yue QL, He CX, Wu MC, Xu JB, Zhao TS. Pack-level modeling of a liquid cooling system for power batteries in electric vehicles. *International Journal of Heat and Mass Transfer* 2022;192:122946.

[61] Janssen DD, Dixon JM, Young SJ, Kulacki FA. Flow Boiling in a Short Narrow Gap Channel. Heat Transfer Summer Conference, vol. 55485, American Society of Mechanical Engineers; 2013, p. V002T07A017.

[62] E J, Yue M, Chen J, Zhu H, Deng Y, Zhu Y, et al. Effects of the different air cooling strategies on cooling performance of a lithium-ion battery module with baffle. *Applied Thermal Engineering* 2018;144:231–41.

[63] Karami A, Nayebi A. Kinematic hardening analysis of Li-ion battery with concentration-dependent material behaviours under cyclic charging and discharging. *Journal of Power Sources* 2020;461:228155.

[64] Wang Y, Li H, Wang Z, Lian C, Xie Z. Factors affecting stress in anode particles during charging process of lithium ion battery. *Journal of Energy Storage* 2021;43:103214.

[65] Shi Y, Guan L, Gao C, Shen A, Chen B, Zhou J, et al. Investigation on high-energy Si anode mechanical-electrochemical-thermal characteristic under wide temperature range. *International Journal of Solids and Structures* 2023;262–263:112046.

[66] Qin P, Liao M, Mei W, Sun J, Wang Q. The experimental and numerical investigation on a hybrid battery thermal management system based on forced-air convection and internal finned structure. *Applied Thermal Engineering* 2021;195:117212.

[67] State-owned Assets Supervision and Administration Commission of the State Council. World's First Immersion Cooling Battery Energy Storage Power Plant Starts Operation 2023.